THE JOURNAL OF PHYSICAL CHEMISTRY LETTERS
A JOURNAL OF THE AMERICAN CHEMICAL SOCIETY

pubs.acs.org/JPCL

Letter

Crystalline Fully Carboxylated Polyacetylene Obtained under High Pressure as a Li-Ion Battery Anode Material

Xuan Wang, Xingyu Tang, Peijie Zhang, Yida Wang, Dexiang Gao, Jie Liu, Kanglong Hui, Yajie Wang, Xiao Dong, Takanori Hattori, Asami Sano-Furukawa, Kazutaka Ikeda, Ping Miao, Xiaohuan Lin, Mingxue Tang, Zicheng Zuo, Haiyan Zheng,* Kuo Li, and Ho-kwang Mao

Cite This: *J. Phys. Chem. Lett.* 2021, 12, 12055−12061

Read Online

ACCESS | Metrics & More | Article Recommendations | Supporting Information

ABSTRACT: Substituted polyacetylene is expected to improve the chemical stability, physical properties, and combine new functions to the polyacetylene backbones, but its diversity is very limited. Here, by applying external pressure on solid acetylenedicarboxylic acid, we report the first crystalline poly-dicarboxylacetylene with every carbon on the *trans*-polyacetylene backbone bonded to a carboxyl group, which is very hard to synthesize by traditional methods. The polymerization is evidenced to be a topochemical reaction with the help of hydrogen bonds. This unique structure combines the extremely high content of carbonyl groups and high conductivity of a polyacetylene backbone, which exhibits a high specific capacity and excellent cycling/rate performance as a Li-ion battery (LIB) anode. We present a completely functionalized crystalline polyacetylene and provide a high-pressure solution for the synthesis of polymeric LIB materials and other polymeric materials with a high content of active groups.

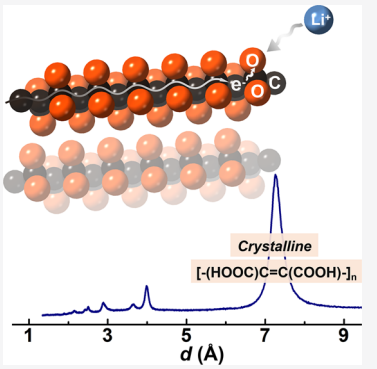

Organic carbonyl compounds have been widely studied as promising electrode materials for lithium-ion batteries (LIBs) because of their availability, easy modification, high theoretical capacity, and fast electrochemical kinetics.[1−4] However, their severe dissolution in electrolytes and low electronic conductivity result in a decline in capacity and significantly restrict the rate performance.[5,6] On the contrary, as the "mother of all" conductive polymers, polyacetylene was investigated first as a polymeric electrode material for rechargeable batteries. Due to the absence of REDOX moieties, the capacity of the polyacetylene is comparably low.[7−9] A solution for avoiding these shortcomings is to bond a large number of carbonyls to conductive polyacetylene backbones,[10−12] and such a combination would optimize the capacity, electronic conductivity, and solubility simultaneously. The volumetric capacity would also be improved for the crystalline polymer.

Poly-acetylenedicarboxylic acid, a fully carboxylated polyacetylene, is thus an ideal candidate for a LIB electrode material with a theoretical capacity of 470 mAh g^{-1}. However, it is difficult to obtain through traditional catalytic synthesis using Ziegler−Natta or other transition metal catalysts,[13−15] because of the electronic and steric effects of the carbonyl groups and inactivation of the catalyst by an acidic proton.[16,17] Only the $MoCl_5$−Ph_4Sn catalyst was reported to catalyze the polymerization of acetylenedicarboxylic acid (ADCA, $C_4H_2O_4$), with a yield of only ∼13% and a molecular weight much lower than 2000.[18] γ-Irradiation was also explored to initiate the polymerization of solid ADCA, but this gave an only 5.5% yield and led to degradation upon overexposure.[19]

High pressure is a robust method for initiating the polymerization of substituted alkynes and producing conductive carbon backbones with the initial composition maintained.[20−25] Even the $C{\equiv}C^{2-}$ anions in CaC_2[26] and Li_2C_2[27,28] can polymerize under high pressure, accompanied by a 10^9-fold enhancement in conductivity. For molecules, upon compression of C_2I_2, a sp^2-C network can be generated with a high content of C−I bonds and a conductivity comparable to that of Br-doped polyacetylene.[29] ADCA was also reported to oligomerize with n = 8 at 6 GPa.[30] In this work, by systematically investigating the pressure-induced polymerization (PIP) of solid ADCA, we obtained crystalline poly-dicarboxylacetylene $[\text{-(HOOC)C}{=}\text{C(COOH)-}]_n$ material, with every carbon on the *trans*-polyacetylene chains uniformly connected to a carboxyl group. This polymer exhibits high specific capacity, excellent cycling stability, and excellent rate performance due to the high-density modification of active groups, enhanced electronic conductivity, and decreased solubility. With a comprehensive experimental and theoretical

Received: November 14, 2021
Accepted: December 9, 2021

Downloaded via BEIJING COMPUTATIONAL SCI RSRCH CTR on December 15, 2021 at 00:01:05 (UTC).
See https://pubs.acs.org/sharingguidelines for options on how to legitimately share published articles.

© XXXX American Chemical Society

https://doi.org/10.1021/acs.jpclett.1c03734
J. Phys. Chem. Lett. 2021, 12, 12055−12061

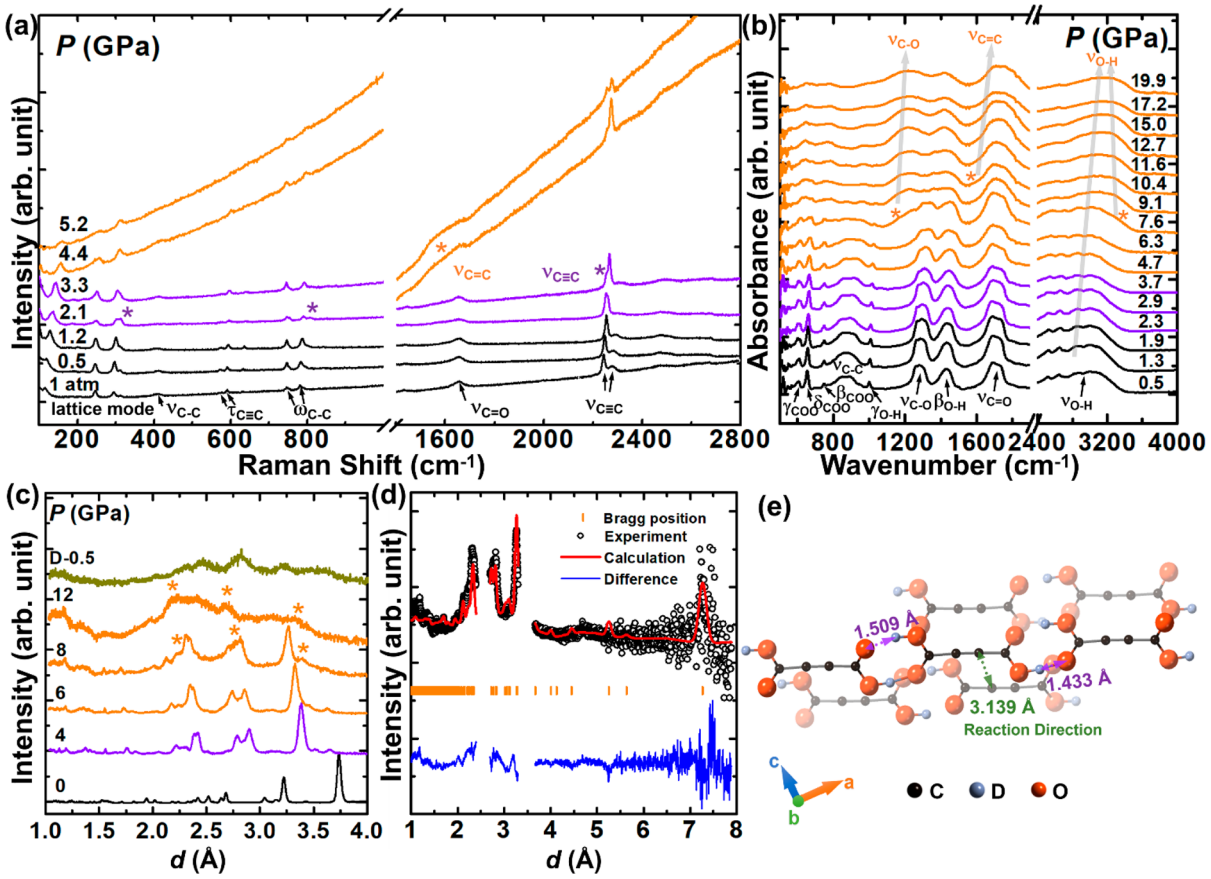

Figure 1. (a) Raman and (b) IR spectra of ADCA under external pressure. The assignments of Raman and IR modes are listed in Tables S1 and S2, respectively. (c) Time-of-flight (TOF) neutron diffraction patterns of ADCA-d_2 upon compression. (d) Rietveld refinement plot and (e) crystal structure of ADCA-d_2 at 8 GPa. The asterisks denote the appearance of new peaks. ν, δ, γ, τ, ω, and β represent the stretching, scissoring, out-of-plane bending, torsion, wagging, and the in-plane bending vibrations, respectively. The green and purple arrows indicate the C···C and O···D distances, respectively.

study of the reaction, the topochemical PIP mechanism and the crystal-to-crystal polymerization process assisted by the H-bond are demonstrated, which provides a novel strategy for synthesizing the crystalline poly-carbonyl electrode materials.

Upon compression, a tiny phase transition (phase I to II) of ADCA [purity checked by powder X-ray diffraction (XRD) with Rietveld refinement as shown in Figure S1] was first observed at ~2 GPa in in situ Raman spectra (Figure 1a and Figure S2). The lattice modes and C−C wagging (ω_{C-C}) mode split, and a new peak at the low-frequency side of C≡C stretching ($\nu_{C\equiv C}$) appeared, which is consistent with the literature.[31] With an increase in pressure, the sample becomes darker. The new peak centered at ~1600 cm^{-1} ascribed to the C═C stretching ($\nu_{C=C}$) is observed, indicating the polymerization of ADCA. In the infrared (IR) absorption spectra, new bands appeared at 1200 and ~3300 cm^{-1} at 7.6 GPa (asterisks in Figure 1b), which are identified as the C−O (ν_{C-O}) and O−H stretching (ν_{O-H}) of the polymer, respectively. Subsequently, the ν_{C-O} and β_{O-H} modes of the ADCA monomer gradually merged at 9.1 GPa. The $\nu_{C=C}$ mode of the product is close to that of the carbonyl group but can be clearly distinguished above 10.4 GPa. During the decompression, the ν_{C-O} and $\nu_{C=C}$ modes were maintained, proving the irreversibility and hence the stability of the polymer at ambient pressure (Figure S3). The β_{O-H} and ν_{O-H} modes are also always present, indicating the stability of the hydrogen bonds.

The Raman and IR results demonstrated the PIP of ADCA. To understand the structural variation upon compression, we performed in situ time-of-flight (TOF) neutron diffraction on deuterated ADCA [ADCA-d_2, $C_4D_2O_4$ (Figure 1c)]. At ambient pressure, ADCA-d_2 has a monoclinic lattice (space group $P2_1/n$). Two hydrogen bonds between the carboxyl groups link molecules to form chains (Figure S4), and the minimum interchain distance between the alkynyls is ~4 Å. During compression, all diffractions moved toward low d spacing, signifying lattice compression. At 4 GPa, the lattice parameters of phase II are similar to those reported in the literature,[30] but space group Pn fits the data better, which allows bent carbon skeletons. The corresponding Rietveld refinement result is shown in Figure S5 and Table S3. At 8 GPa, several new peaks appeared (asterisks in Figure 1c), corresponding to the PIP of ADCA-d_2. By performing the Rietveld refinement on the remaining peaks of the ADCA-d_2 monomer (Figure 1d,e), we determined its "critical structure" before PIP. The lengths of the C≡C (1.191 Å) and C−C (1.390 Å) bonds did not change significantly, while the shortest hydrogen bond was compressed gradually to a $d_{O\cdots D}$ of 1.43 Å at 8 GPa (Table S4); the intermolecular distance between alkynyl groups ($d_{C\cdots C}$) was compressed to 3.1 Å, along the $b - c/b + c$ direction. This distance agrees with the reaction threshold of many alkynyl compounds under high pressure, like the $d_{C\cdots C}$ of 3.1 Å at ~5 GPa for acetylene,[32] the $d_{C\cdots C}$ of 3.0 Å at ~13 GPa for NaCCH,[33] and the $d_{C\cdots C}$ of 2.9 Å

https://doi.org/10.1021/acs.jpclett.1c03734
J. Phys. Chem. Lett. 2021, 12, 12055−12061

at ~20 GPa for CaC_2,[26] which suggests the C≡C bonding may happen along the $b - c/b + c$ direction. Above 12 GPa, the reaction is complete, and the polymer can be recovered under ambient conditions (Figure 1c).

To understand the bonding process, we performed metadynamic simulation with a $2a \times 2b \times 1c$ supercell of ADCA. At 300 K and 9 GPa, the alkyne groups start to approach each other and bend, as shown in Figure 2 (step 47).

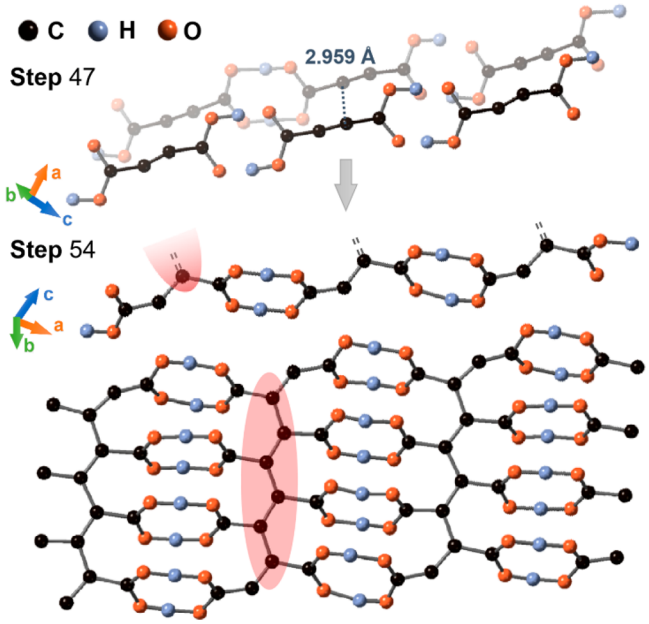

Figure 2. Metadynamic simulation of ADCA at 300 K and 9 GPa. The step numbers represent the generation numbers. The red shadows indicate the C═C/C−C chain.

Then, the neighboring alkyne carbon atoms bond to form tetramers with the *trans*-polyacetylene skeleton along the $b-c$ direction (step 54, marked by a red shadow). This fully agrees with the experimental results exhibited in the neutron data and the proposed topochemical bonding process.

For further investigation, we synthesized several samples by Paris−Edinburgh (PE) press at 8, 10, and 16 GPa (denoted PE-8, PE-10, and PE-16, respectively). Sharp diffractions (marked by the triangles) are clearly observed in the XRD pattern, which unambiguously demonstrates that the obtained poly-ADCA is crystalline (Figure 3a). Compared with the XRD pattern of ADCA, the unreacted ADCA is still present in PE-8 and PE-10, but not in PE-16. On the basis of the Rietveld refinement of ADCA and poly-ADCA discussed below, the ratio of ADCA to product was determined. Both the synthetic pressure and the reaction time will affect the yield (Figure S6). When the ADCA is kept at 8 and 10 GPa for 24 h, the yields are 30.7% and 38.0%, respectively. With an increase in reaction time from 12 to 48 h at 10 GPa, the yield increased from 28.8% to 39.2%. Considering the balance between the time and the yield, we chose 10 GPa and 24 h to synthesize the sample for the battery measurement as described in the following. After the unreacted ADCA/oligomers had been removed from PE-10 by washing with ethanol (labeled PE-10-washed), the IR (Figure S7) and XRD data show the product is consistent with PE-16. The molecular weights of PE-10-washed and PE-16 were determined by gel permeation chromatography (GPC), which shows the molecular weight ($\bar{M}_n$) of PE-16 is 2.2×10^4

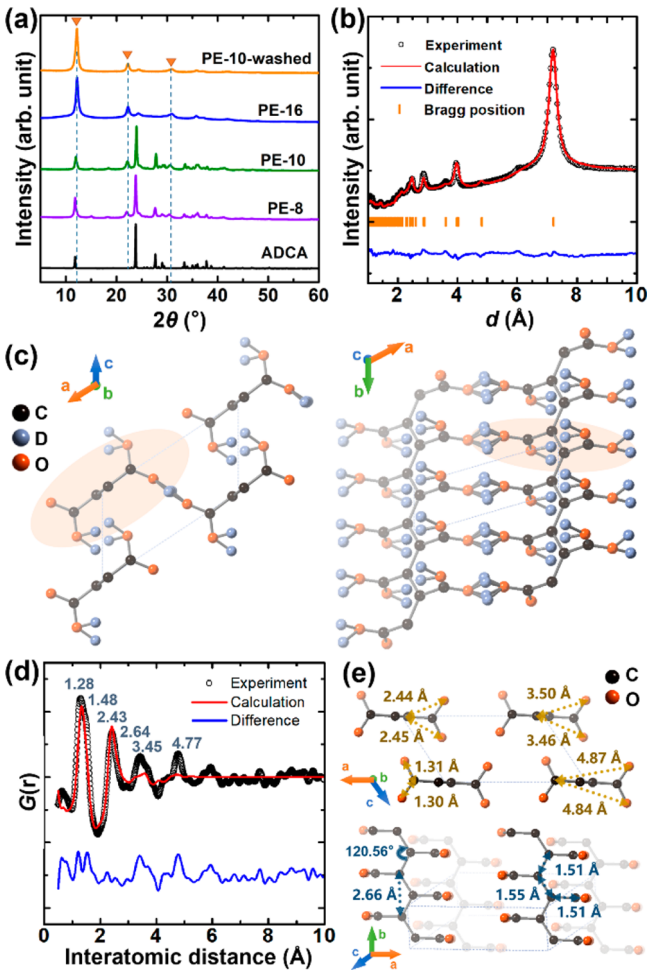

Figure 3. (a) XRD patterns of PE-8, PE-10, PE-10-washed, PE-16, and ADCA. PE-8, PE-10, and PE-16 represent the polymers synthesized at 8, 10, and 16 GPa, respectively, for 24 h by using PE press. PE-10-washed represents PE-10 after the unreacted ADCA and oligomers had been removed by washing with ethanol. (b) Rietveld refinement plot of the neutron diffraction pattern of PE-16-d_2. (c) Crystal structure of PE-16-d_2 along the b and c axes. (d) Neutron PDF experiment data of PE-16-d_2 and the fitting result. (e) Interatomic distances of C and O atoms in the local structure of the product. The D atom has been omitted for the sake of clarity.

with a degree of polymerization ($\bar{X}_n$) of ~193, slightly higher than those of PE-10-washed [$\bar{M}_n = 2.0 \times 10^4$, and $\bar{X}_n = 175$ (Table S5)].

The neutron diffraction data of PE-16-d_2 were collected (Figure 3b), and a unit cell of $a_p = 8.652(7)$ Å, $b_p = 2.663(3)$ Å, $c_p = 5.112(14)$ Å, $\alpha = 109.6(4)°$, $\beta = 119.69(9)°$, and $\gamma = 93.6(3)°$ was found to index the pattern perfectly, which is related to the lattice of the ADCA monomer by relations of approximately $a_p = 0.5a_m - 0.5c_m$, $b_p = 0.5b_m - 0.5c_m$, and $c_p = 0.5b_m + 0.5c_m$. The crystal structure of the polymer was then proposed on the basis of the structure of ADCA obtained at 8 GPa and the metadynamic simulation. Rietveld refinement was then performed using the neutron diffraction data (Figure 3b), and the crystal structure as well as the Rietveld refinement results of the polymer is shown in Figure 3c and Tables S6 and S7, respectively. The PIP-ADCA has parallelly stacked *trans*-polyacetylene chains along the b axis. The C═C bonds are conjugated with bond lengths of 1.51 Å and a C−C−C bond angle of 121°, similar to that in *trans*-polyacetylene (Figure

https://doi.org/10.1021/acs.jpclett.1c03734
J. Phys. Chem. Lett. 2021, 12, 12055−12061

S8).[34] Every carbon atom in this chain is connected to a carboxyl group, with its plane perpendicular to the chain. The polyacetylene chains are hence protected by the carboxyl group and then connected by side-to-side hydrogen bonds that are approximately perpendicular to the chain plane, resulting in a network of polymers. This is the key to maintaining the ordered aggregation and obtaining crystalline polymeric products. Compared with the head-to-head hydrogen bonds proposed in the simulation results (Figure 2), the hydrogen bonds in the structure obtained from Rietveld refinement adopt side-to-side geometry, which has a more reasonable range of interchain O···O distances of hydrogen bonds and lower energy [Figure S9; the energy of the polymer with a side-to-side hydrogen bond connection model is lower than that of the head-to-head model by ~24 kJ/mol ($C_4O_4H_2$)].

The neutron pair distribution function (PDF) was also used to examine the local structure of the product. In the $G(r)$ plot (Figure 3d), the peaks at 1.28 and 1.48 Å are attributed to the conjugated C−(═)O and C−(═)C bonds, while the peaks at 2.43 and 2.64 Å are ascribed to the distance between O and its neighboring carbon and that between C and its neighboring carbon in the polyacetylene skeleton, respectively, as shown in Figure 3e. The structure (Table S8) fitted the $G(r)$ data well, with a subtle change in the lattice parameter [a = 8.705(17) Å, b = 2.3859(16) Å, c = 5.364(16) Å, α = 102.86(15)°, β = 123.97(11)°, and γ = 93.6(2)°], which further confirmed the structural model.

The conductivity of PE-16 was achieved by measuring the AC impedance spectrum as shown in Figure 4. An equivalent

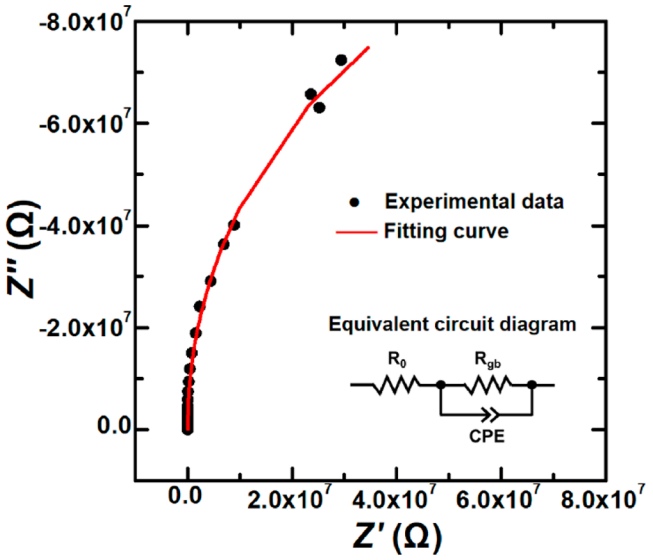

Figure 4. AC impedance spectrum of PE-16 in the Nyquist plot. The equivalent circuit used for fitting is shown in the inset.

circuit shown in the inset was used to fit the Nyquist plot. The permittivity of the semicircle is 2.87 × 10^{-11} F cm^{-1} and is attributed to the grain boundary.[35,36] The corresponding conductivity is 4.54 × 10^{-9} S cm^{-1}, much higher than those of other organic electrode materials, such as 2.36 × 10^{-11} S cm^{-1} for 1,4-naphthoquinone[37] and 1.78 × 10^{-13} S cm^{-1} for triquinoxalinylenes.[38] This is due to the parallel arrangement of the polyacetylene backbone, which facilitates electron migration.

Due to the limited amount of PE-16, we chose PE-10-washed to investigate the electrochemical performance as a LIB anode material. To rule out the influence of the conducting agent, the electrode for cyclic voltammogram (CV) measurement was fabricated by pressing a mixture of 90 wt % PE-10-washed and 10 wt % polytetrafluoroethylene (PTFE) on Ni foam. The CV profiles are shown in Figure 5a,

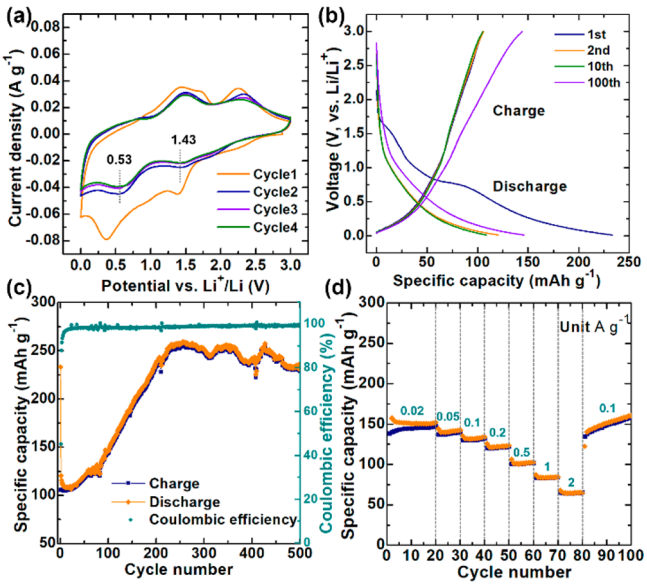

Figure 5. (a) Cyclic voltammograms at a scan rate of 0.5 mV s^{-1}. (b) Galvanostatic discharge−charge profiles and (c) electrochemical cycling performance at a current density of 0.1 A g^{-1}. (d) Rate performance under different current densities (amperes per gram).

and two cathodic peaks are observed at ~0.53 and ~1.43 V, which correspond to the reduction of carbonyl groups upon insertion of Li^+.[5] The sharp reduction peak at 0.36 V is obvious in the first cycle and less pronounced in the following cycles, which is characteristic of the formation of the solid electrolyte interface (SEI) layer at the lower potential range and the irreversible bonding of Li^+ ions to the carboxyl groups. This is consistent with the first charge−discharge profile shown in Figure 5b, which reveals the initial discharge and charge capacities to be 233.2 and 105.5 mAh g^{-1}, respectively, corresponding to a Coulombic efficiency of 45.22%. Fortunately, its Coulombic efficiency increases dramatically upon cycling, reaching over 95% after five cycles and exceeding 98% after 25 cycles (Figure 5c), suggesting that the insertion and release of Li ions in each cycle become equal. Moreover, the discharge−charge capacity of the polymer electrode gradually increased after the 10th cycle and reached the maximum specific capacity of 259.3 mAh g^{-1} at the 256th cycle. This indicates the continuous activation of the poly-ADCA material with the charge−discharge cycles.[39−41] The LIB can maintain a capacity of ~240 mAh g^{-1} in the subsequent cycles. After 500 cycles, a high specific capacity of approximately 230.3 mAh g^{-1} is still obtained with a Coulombic efficiency around 99.5%, which demonstrates the excellent cycling stability of the PIP-ADCA electrode.

We further evaluated the rate performance of PE-10-washed (Figure 5d). The electrode delivers initial reversible capacities of 152, 141, 132, 122, 102, 84, and 65 mAh g^{-1} at current rates of 0.02, 0.05, 0.1, 0.2, 0.5, 1, and 2 A g^{-1} after 20 (or 10) cycles, respectively. When the applied current density is

https://doi.org/10.1021/acs.jpclett.1c03734
J. Phys. Chem. Lett. 2021, 12, 12055−12061

decreased to 0.1 A g^{-1}, a discharge capacity of 169.1 mAh g^{-1} is recovered, reflecting good rate performance and structural stability of the poly-ADCA. Hence, we can conclude that in poly-ADCA, the high content of carbonyl groups on the polyacetylene backbone is beneficial for its excellent electrochemical performance in terms of high reversible capacity, long cycling stability, and good rate performance.

In conclusion, by applying external pressure on ADCA, we synthesized crystalline poly-dicarboxylacetylene [-(HOOC)-C═C(COOH)-]$_n$ and investigated its application in Li-ion anode materials. Solid ADCA experienced a topochemical polymerization process, with its C≡C bonds bonding to each other along the *b*−*c* direction, and generated *trans*-polyacetylene chains with every carbon atom connected to a carboxyl group. The intermolecular hydrogen bonds play a key role in maintaining the crystallinity of the PIP product, and its atomic positions can be determined by Rietveld refinement. The product also retains carboxyl groups as REDOX groups, with reduced solubility and improved electrical conductivity due to the conjugated backbone. This makes it a potential LIB anode material with high specific capacity, excellent cycle stability, and excellent rate performance. Our study provides a high-pressure route for the tailored synthesis of polymeric Li-ion battery materials with a high content of REDOX active groups, which has no precedent. Via introduction of specific functional groups into the reactant and by following this topochemical PIP strategy, more polymeric materials with designed functions can be expected.

■ ASSOCIATED CONTENT

Supporting Information

The Supporting Information is available free of charge at https://pubs.acs.org/doi/10.1021/acs.jpclett.1c03734.

Experimental procedures, in situ high-pressure Raman and infrared absorption spectra of ADCA, in situ time-of-flight neutron diffraction of ADCA and determination of crystal structures under high pressure, synthesis and characterization of polymers, computational details of the metadynamics simulation, AC impedance spectroscopy of PE-16, cyclic voltammetry and lithium-ion battery performance of PE-10-washed, Figures S1−S9, and Tables S1−S8 (PDF)

■ AUTHOR INFORMATION

Corresponding Author

Haiyan Zheng − *Center for High Pressure Science and Technology Advanced Research, Beijing 100094, P. R. China;* orcid.org/0000-0002-4727-5912; Email: zhenghy@hpstar.ac.cn

Authors

Xuan Wang − *Center for High Pressure Science and Technology Advanced Research, Beijing 100094, P. R. China*

Xingyu Tang − *Center for High Pressure Science and Technology Advanced Research, Beijing 100094, P. R. China*

Peijie Zhang − *Center for High Pressure Science and Technology Advanced Research, Beijing 100094, P. R. China;* orcid.org/0000-0001-6355-5482

Yida Wang − *Center for High Pressure Science and Technology Advanced Research, Beijing 100094, P. R. China*

Dexiang Gao − *Center for High Pressure Science and Technology Advanced Research, Beijing 100094, P. R. China*

Jie Liu − *Center for High Pressure Science and Technology Advanced Research, Beijing 100094, P. R. China*

Kanglong Hui − *Center for High Pressure Science and Technology Advanced Research, Beijing 100094, P. R. China*

Yajie Wang − *Center for High Pressure Science and Technology Advanced Research, Beijing 100094, P. R. China*

Xiao Dong − *Key Laboratory of Weak-Light Nonlinear Photonics and School of Physics, Nankai University, Tianjin 300071, P. R. China*

Takanori Hattori − *J-PARC Center, Japan Atomic Energy Agency, Tokai, Ibaraki 319-1195, Japan*

Asami Sano-Furukawa − *J-PARC Center, Japan Atomic Energy Agency, Tokai, Ibaraki 319-1195, Japan*

Kazutaka Ikeda − *Institute of Materials Structure Science, High Energy Accelerator Research Organization (KEK), Tsukuba, Ibaraki 305-0801, Japan*

Ping Miao − *Institute of Materials Structure Science, High Energy Accelerator Research Organization (KEK), Tokai, Ibaraki 319-1106, Japan; Institute of High Energy Physics, Chinese Academy of Sciences, Beijing 100049, P. R. China; Spallation Neutron Source Science Center, Dongguan 523803, P. R. China;* orcid.org/0000-0003-1937-1736

Xiaohuan Lin − *Center for High Pressure Science and Technology Advanced Research, Beijing 100094, P. R. China*

Mingxue Tang − *Center for High Pressure Science and Technology Advanced Research, Beijing 100094, P. R. China;* orcid.org/0000-0002-7282-4100

Zicheng Zuo − *CAS Key Laboratory of Organic Solids, Institute of Chemistry, Chinese Academy of Sciences, Beijing 100190, P. R. China;* orcid.org/0000-0001-7002-9886

Kuo Li − *Center for High Pressure Science and Technology Advanced Research, Beijing 100094, P. R. China;* orcid.org/0000-0002-4859-6099

Ho-kwang Mao − *Center for High Pressure Science and Technology Advanced Research, Beijing 100094, P. R. China*

Complete contact information is available at: https://pubs.acs.org/10.1021/acs.jpclett.1c03734

Notes

The authors declare no competing financial interest.

■ ACKNOWLEDGMENTS

The authors acknowledge the support of the National Natural Science Foundation of China (NSFC) (Grants 21875006, 22022101, and 21771011). The authors also acknowledge the support of the National Key Research and Development Program of China (2019YFA0708502). X.D. is thankful for the support from NSFC (21803033) and the Young Elite Scientists Sponsorship Program by Tianjin (TJSQNTJ-2018-18). Neutron diffraction experiments at J-PARC were performed through the J-PARC user programs (2018B0249 and 2018BF2106). This research used resources at the Spallation Neutron Source, a U.S. Department of Energy Office of Science User Facility operated by the Oak Ridge National Laboratory. The calculations were performed on the TianheII supercomputer at the Chinese National Supercomputer Center in Guangzhou. The authors thank Dr. Wenyun Yang and Xiaobai Ma for help with the in situ neutron diffraction experiments at HRPD of the China Advanced Research Reactor (CARR). The authors thank Drs. Leiming Fang, Lei Xie, and Xiping Chen for their help with the in situ neutron diffraction experiments at the Fenghuang diffractom-

eter of the China Mianyang Research Reactor (CMRR). The authors also thank Dr. Xiaodong Yin of the Beijing Institute of Technology for his discussion about the CV measurement of PE-10-washed.

REFERENCES

(1) Lu, Y.; Chen, J. Prospects of Organic Electrode Materials for Practical Lithium Batteries. *Nature Rev. Chem.* **2020**, *4*, 127−142.
(2) Ma, C.; Zhao, X.; Kang, L.; Wang, K.-X.; Chen, J.-S.; Zhang, W.; Liu, J. Non-Conjugated Dicarboxylate Anode Materials for Electrochemical Cells. *Angew. Chem., Int. Ed.* **2018**, *57*, 8865−8870.
(3) Esser, B.; Dolhem, F.; Becuwe, M.; Poizot, P.; Vlad, A.; Brandell, D. A Perspective on Organic Electrode Materials and Technologies for Next Generation Batteries. *J. Power Sources* **2021**, *482*, 228814.
(4) Lu, Y.; Zhang, Q.; Li, L.; Niu, Z.; Chen, J. Design Strategies toward Enhancing the Performance of Organic Electrode Materials in Metal-Ion Batteries. *Chem.* **2018**, *4*, 2786−2813.
(5) Heiska, J.; Nisula, M.; Karppinen, M. Organic Electrode Materials with Solid-State Battery Technology. *J. Mater. Chem. A* **2019**, *7*, 18735−18758.
(6) Oubaha, H.; Gohy, J.-F.; Melinte, S. Carbonyl-Based π-Conjugated Materials: from Synthesis to Applications in Lithium-Ion Batteries. *ChemPlusChem* **2019**, *84*, 1179−1214.
(7) Macinnes, D., Jr; Druy, M. A.; Nigrey, P. J.; Nairns, D. P.; Macdiarmid, A. G.; Heeger, A. J. Organic Batteries: Reversible *n*- and *p*-Type Electrochemical Doping of Polyacetylene, $(CH)_x$. *J. Chem. Soc., Chem. Commun.* **1981**, 317−319.
(8) Hager, M. D.; Esser, B.; Feng, X.; Schuhmann, W.; Theato, P.; Schubert, U. S. Polymer-Based Batteries-Flexible and Thin Energy Storage Systems. *Adv. Mater.* **2020**, *32*, 2000587.
(9) Novák, P.; Müller, K.; Santhanam, K. S. V.; Haas, O. Electrochemically Active Polymers for Rechargeable Batteries. *Chem. Rev.* **1997**, *97*, 207−281.
(10) Basescu, N.; Liu, Z.-X.; Moses, D.; Heeger, A. J.; Naarmann, H.; Theophilou, N. High Electrical Conductivity in Doped Polyacetylene. *Nature* **1987**, *327*, 403−405.
(11) Heeger, A. J. Nobel Lecture: Semiconducting and Metallic Polymers: The Fourth Generation of Polymeric Materials. *Rev. Mod. Phys.* **2001**, *73*, 681.
(12) Chiang, C. K.; Fincher, C. R., Jr; Park, Y. W.; Heeger, A. J.; Shirakawa, H.; Louis, E. J.; Gau, S. C.; MacDiarmid, A. G. Electrical Conductivity in Doped Polyacetylene. *Phys. Rev. Lett.* **1977**, *39*, 1098−1101.
(13) Masuda, T. Substituted Polyacetylenes: Synthesis, Properties, and Functions. *Polym. Rev.* **2017**, *57*, 1−14.
(14) Saito, M. A.; Maeda, K.; Onouchi, H.; Yashima, E. Synthesis and Macromolecular Helicity Induction of a Stereoregular Polyacetylene Bearing a Carboxy Group with Natural Amino Acids in Water. *Macromolecules* **2000**, *33*, 4616−4618.
(15) Maeda, K.; Goto, H.; Yashima, E. Stereospecific Polymerization of Propiolic Acid with Rhodium Complexes in the Presence of Bases and Helix Induction on the Polymer in Water. *Macromolecules* **2001**, *34*, 1160−1164.
(16) Lam, J. W. Y.; Luo, J.; Dong, Y.; Cheuk, K. K. L.; Tang, B. Functional Polyacetylenes: Synthesis, Thermal Stability, Liquid Crystallinity, and Light Emission of Polypropiolates. *Macromolecules* **2002**, *35*, 8288−8299.
(17) Kishimoto, Y.; Eckerle, P.; Miyatake, T.; Kainosho, M.; Ono, A.; Ikariya, T.; Noyori, R. Well-Controlled Polymerization of Phenylacetylenes with Organorhodium(I) Complexes: Mechanism and Structure of the Polyenes. *J. Am. Chem. Soc.* **1999**, *121*, 12035−12044.
(18) Masuda, T.; Kawai, M.; Higashimura, T. Polymerization of Propiolic Acid and its Derivatives Catalysed by $MoCl_5$. *Polymer* **1982**, *23*, 744−747.
(19) Usanmaz, A.; Altürk, E. Radiation Induced Solid-State Polymerization of Acetylenedicarboxylic Acid. *J. Macromol. Sci., Part A: Pure Appl. Chem.* **2002**, *39*, 379−395.
(20) Wang, X.; Li, K.; Zheng, H.; Zhang, P. Chemical Reactions of Molecules under High Pressure. *Chem. Bull.* **2019**, *82*, 387−398.
(21) Zhang, P.; Tang, X.; Wang, Y.; Wang, X.; Gao, D.; Li, Y.; Zheng, H.; Wang, Y.; Wang, X.; Fu, R.; Tang, M.; Ikeda, K.; Miao, P.; Hattori, T.; Sano-Furukawa, A.; Tulk, C. A.; Molaison, J. J.; Dong, X.; Li, K.; Ju, J.; Mao, H.-k. "Distance Selected" Topochemical Dehydro-Diels-Alder Reaction of 1,4-Diphenylbutadiyne towards Crystalline Graphitic Nanoribbons. *J. Am. Chem. Soc.* **2020**, *142*, 17662−17669.
(22) Yoo, C.-S. Chemistry under Extreme Conditions: Pressure Evolution of Chemical Bonding and Structure in Dense Solids. *Matter Radiat. Extrem.* **2020**, *5*, 018202.
(23) Yang, X.; Wang, X.; Wang, Y. D.; Li, K.; Zheng, H. From Molecules to Carbon Materials-High Pressure Induced Polymerization and Bonding Mechanisms of Unsaturated Compounds. *Crystals* **2019**, *9*, 490.
(24) Wilhelm, C.; Boyd, S. A.; Chawda, S.; Fowler, F. W.; Goroff, N. S.; Halada, G. P.; Grey, C. P.; Lauher, J. W.; Luo, L.; Martin, C. D.; Parise, J. B.; Tarabrella, C.; Webb, J. A. Pressure-Induced Polymerization of Diiodobutadiyne in Assembled Cocrystals. *J. Am. Chem. Soc.* **2008**, *130*, 4415−4420.
(25) Jin, H.; Plonka, A. M.; Parise, J. B.; Goroff, N. S. Pressure Induced Topochemical Polymerization of Diiodobutadiyne: a Single-Crystal-to-Single-Crystal Transformation. *CrystEngComm* **2013**, *15*, 3106−3110.
(26) Zheng, H.; Wang, L.; Li, K.; Yang, Y.; Wang, Y.; Wu, J.; Dong, X.; Wang, C.-H.; Tulk, C. A.; Molaison, J. J.; Ivanov, I. N.; Feygenson, M.; Yang, W.; Guthrie, M.; Zhao, Y.; Mao, H. K.; Jin, C. Pressure Induced Polymerization of Acetylide Anions in CaC_2 and 10^7 Fold Enhancement of Electrical Conductivity. *Chem. Sci.* **2017**, *8*, 298−304.
(27) Dong, X.; Wang, L.; Li, K.; Zheng, H.; Wang, Y.; Meng, Y.; Shu, H.; Mao, H.-k.; Feng, S.; Jin, C. Tailored Synthesis of the Narrowest Zigzag Graphene Nanoribbon Structure by Compressing the Lithium Acetylide under High Temperature. *J. Phys. Chem. C* **2018**, *122*, 20506−20512.
(28) Wang, L.; Dong, X.; Wang, Y.; Zheng, H.; Li, K.; Peng, X.; Mao, H.-k.; Jin, C.; Meng, Y.; Huang, M.; Zhao, Z. Pressure-Induced Polymerization and Disproportionation of Li_2C_2 Accompanied with Irreversible Conductivity Enhancement. *J. Phys. Chem. Lett.* **2017**, *8*, 4241−4245.
(29) Ward, M. D.; Huang, H.-T.; Zhu, L.; Popov, D.; Strobel, T. A. High-Pressure Behavior of C_2I_2 and Polymerization to a Conductive Polymer. *J. Phys. Chem. C* **2019**, *123*, 11369−11377.
(30) Delori, A.; Hutchison, I. B.; Bull, C. L.; Funnell, N. P.; Urquhart, A. J.; Oswald, I. D. H. Reaction of Acetylenedicarboxylic Acid Made Easy: High-Pressure Route for Polymerization. *Cryst. Growth Des.* **2018**, *18*, 1425−1431.
(31) Yue, M.; Wang, Y.; Wang, L.; Lin, X.; Li, K.; Zheng, H.; Yang, T. Pressure-Induced Polymerization of Butyndioic Acid and its Li^+ Salt. *Chin. Chem. Lett.* **2018**, *29*, 328−330.
(32) Sun, J.; Dong, X.; Wang, Y.; Li, K.; Zheng, H.; Wang, L.; Cody, G. D.; Tulk, C. A.; Molaison, J. J.; Lin, X.; Meng, Y.; Jin, C.; Mao, H.-k. Pressure-Induced Polymerization of Acetylene: Structure-Directed Stereoselectivity and a Possible Route to Graphane. *Angew. Chem., Int. Ed.* **2017**, *56*, 6553−6557.
(33) Han, J.; Tang, X.; Wang, Y.; Wang, Y.; Han, Y.; Lin, X.; Dong, X.; Lee, H.; Zheng, H.; Li, K.; Mao, H.-K. Pressure-Induced Polymerization of Monosodium Acetylide: a Radical Reaction Initiated Topochemically. *J. Phys. Chem. C* **2019**, *123*, 30746−30753.
(34) Shimamura, K.; Karasz, F. E.; Hirsch, J. A.; Chien, J. C. W. Crystal Structure of Trans-polyacetylene. *Makromol. Chem., Rapid Commun.* **1981**, *2*, 473−480.
(35) Sinclair, D. C. Characterization of Electro-Materials Using AC Impedance Spectroscopy. *Bol. Soc. Esp. Ceram. Vidrio* **1995**, *34*, 55−65.
(36) Irvine, J. T. S.; Sinclair, D. C.; West, A. R. Electroceramics: Characterization by Impedance Spectroscopy. *Adv. Mater.* **1990**, *2*, 132−138.

https://doi.org/10.1021/acs.jpclett.1c03734
J. Phys. Chem. Lett. 2021, 12, 12055−12061

(37) Lee, J.; Park, M. J. Tattooing Dye as a Green Electrode Material for Lithium Batteries. *Adv. Energy Mater.* **2017**, *7*, 1602279.
(38) Matsunaga, T.; Kubota, T.; Sugimoto, T.; Satoh, M. High-Performance Lithium Secondary Batteries Using Cathode Active Materials of Triquinoxalinylenes Exhibiting Six Electron Migration. *Chem. Lett.* **2011**, *40*, 750−752.
(39) Park, J.; Lee, C. W.; Joo, S. H.; Park, J. H.; Hwang, C.; Song, H.-K.; Park, Y. S.; Kwak, S. K.; Ahn, S.; Kang, S. J. Contorted Polycyclic Aromatic Hydrocarbon: Promising Li Insertion Organic Anode. *J. Mater. Chem. A* **2018**, *6*, 12589−12597.
(40) Xu, J.; Mahmood, J.; Dou, Y.; Dou, S.; Li, F.; Dai, L.; Baek, J.-B. 2D Frameworks of C_2N and C_3N as New Anode Materials for Lithium-Ion Batteries. *Adv. Mater.* **2017**, *29*, 1702007.
(41) Kim, E.; Kim, H.; Park, B.-J.; Han, Y.-H.; Park, J. H.; Cho, J.; Lee, S.-S.; Son, J. G. Etching-Assisted Crumpled Graphene Wrapped Spiky Iron Oxide Particles for High-Performance Li-Ion Hybrid Supercapacitor. *Small* **2018**, *14*, 1704209.

https://doi.org/10.1021/acs.jpclett.1c03734
J. Phys. Chem. Lett. 2021, 12, 12055−12061